obtain perturbations in state, and the series expansion Eq. (9) to determine the thrust direction schedule. This series is expanded about the junction points of the impulsive transfer arc, subsequent iterations use an expansion about the burn begin times, $t_B$. 2) The coast arc succeeding each burn is determined by projecting the burn end conditions via the two-body transition matrix[7] to the initial time of the following burn. 3) Next, a matrix of influence coefficients is numerically generated which relates small changes in the components of the primer and its time derivative at the initial point of the transfer, i.e., at time $t_I$, to changes in state at the final point of the trajectory at time $t_F$. By individually varying the components of $\mathbf{p}$ and $\dot{\mathbf{p}}$ at $t_I$ and recording the resultant change of the terminal state error, this matrix can be easily generated. 4) From the transfer end point errors $\delta\mathbf{x}^*(t_F)$ of the finite-thrust transfer, appropriate corrections to the components of $\mathbf{p}$ and $\dot{\mathbf{p}}$ at $t_I$ for the next iteration are calculated upon inversion of the matrix developed in the preceding step

$$\delta\mathbf{p}^*(t_I) = -\left(\frac{\partial\mathbf{x}^*(t_F)}{\partial\mathbf{p}^*(t_I)}\right)^{-1}\delta\mathbf{x}^*(t_F) \qquad (16)$$

5) Finally, these corrections are applied to the series describing the burn arc thrust direction schedules. Then the nominal trajectory is updated and the calculation sequence repeated. Burn cutoff times for the second and subsequent iterations are determined by the switching function Eq. (14). The iteration process converges to an optimum finite-thrust transfer trajectory while observing optimality criteria along the path at all times.

### Sample Application

To illustrate the validity of the approach, a Hohmann transfer is considered. Figure 1 shows the excess characteristic speed required when replacing the two thrust impulses by finite-thrust burn arcs, as determined by this method.[8] The excess characteristic speed $\Delta V$ is presented here as a function of the orbit radius ratio $r_2/r_1$ with the initial rocket thrust acceleration as a parameter. As expected, lower initial rocket accelerations give rise to greater fuel penalties since the burn arcs replacing the impulses grow longer resulting in more work which has to be done against gravity and which is not accounted for in the impulsive solution. For this particular application, gravity losses are quite small since the optimum burn arcs are executed at nearly constant radius from the force center. The salient features of nonzero periods of thrust application are, however, apparent. The situation will of course change when transfers with significant radius excursions during the powered phases are encountered.

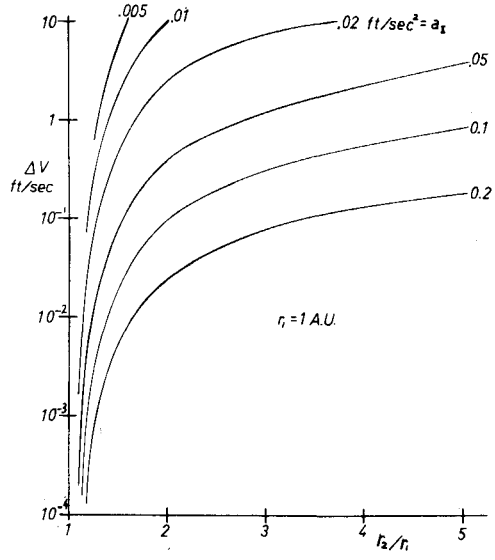


**Fig. 1 Characteristic speed increment due to finite-thrust for Hohmann transfer.**

### References


[1] Lawden, D. F., *Optimal Trajectories for Space Navigation*, Butterworths, London, 1963.

[2] Marchal, C., Marec, J. and Winn, C. B., "Synthèse des Resultats Analytiques sur les Transferts Optimaux Entre Orbites Keplériennes," TP 515, 1967, ONERA, Châtillon, France.

[3] Hazelrigg, G. A., Jr., "An Analytic Study of Multi-Burn Space Trajectories," AMS Rept. 717ad, Jan. 15, 1969, Princeton Univ., Princeton, N.J.

[4] Athans, M. and Falb, P. L., *Optimal Control*, McGraw-Hill, New York, 1966, pp. 125–132.

[5] Robbins, H. M., "An Analytical Study of the Impulsive Approximation," *AIAA Journal*, Vol. 4, No. 8, Aug. 1966, pp. 1417–1423.

[6] Pitkin, E. T., "Second Transition Partial Derivatives Via Universal Variables," *Journal of the Astronautical Sciences*, Vol. 8, 1966, pp. 204–207.

[7] Pitkin, E. T., "Subroutine UCONIC, A Universal Conic Orbit Solution with Partial and Perturbative Derivatives," IBM Contributed Program Library 360D-17.7.001, 1969, IBM Corp., Hawthorne, N.Y.

[8] Grund, E., "Development of Optimal Finite-Thrust Orbit Transfers from Known Impulsive Solutions," Ph.D. dissertation, 1969; Univ. of Connecticut, Storrs, Conn.

[9] Gobetz, F. W. and Doll, J. R., "A Survey of Impulsive Trajectories," *AIAA Journal*, Vol. 7, No. 5, May 1969, pp. 801–834.

[10] Small, H. W., "Minimum N-Impulse Time-Free Transfers Between Elliptic Orbits," *AIAA Journal*, Vol. 9, No. 4, April 1971, pp. 594–599.


# Influence of Helical Serrations on the Aerodynamic Properties of a Spinning Body


MAURICE A. SYLVESTER*

*U.S. Army Ballistic Research Laboratories, Aberdeen Proving Ground, Md.*


### Nomenclature

| | |
|---|---|
| $C_y$ | = yaw force coefficient |
| $d$ | = model diameter |
| $M$ | = Mach number |
| $p$ | = model rotational speed |
| $pd/V$ | = nondimensional spin rate |
| $pd/V = 2\tan\delta_g$ | = matchspin |
| $pd/V > 2\tan\delta_g$ | = overspin |
| $pd/V < 2\tan\delta_g$ | = underspin |
| $Re_l$ | = Reynolds number based on model length and freestream conditions |
| $V$ | = freestream velocity |
| $\alpha$ | = angle of attack |
| $\delta_g$ | = serration angle (angle between the model longitudinal axis and the developed helix) |

### Introduction

DISCREPANCIES have been noted between the observed stability behavior of bullets at long ranges and that predicted from analyses based on the linearized equations of symmetric missiles.[1] Experiments in the Ballistic Research Laboratories' supersonic wind tunnel and range suggest that this behavior may be due to subtle effects of the helical engraving.[2] Deviations from mirror symmetry have been considered previously,[3] but primarily for the more prominent case of finned projectiles. As far as is known, the influence of less prominent grooving has rarely been investigated. This Note presents a sampling of some results from experimental wind-tunnel tests on models with helical serrations.


Presented as Paper 70-557 at the AIAA Atmospheric Flight Mechanics Conference, Tullahoma, Tenn., May 13–15, 1970; submitted July 19, 1971; revision received September 29, 1971.

Index categories: Rocket Vehicle Aerodynamics; Airplane and Component Aerodynamics; Aircraft and Component Wind Tunnel Testing.



* Supervisory Aerospace Engineer.

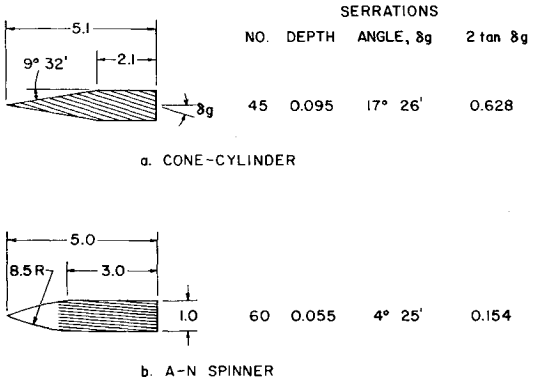


**Fig. 1 Wind-tunnel models (dimensions in calibers, 1 caliber = 2 in.).**

### Test Facility and Models

The tests were conducted in the BRL Supersonic Wind Tunnel at Mach numbers of 1.5 and 2.0 and covered ranges of angle of attack, Reynolds number and spin mismatch which included values typical of bullet conditions. The wind-tunnel models are shown in Fig. 1 along with some of the serration characteristics. The accentuated serrations (as compared with actual bullet engraving) were deemed desirable in these initial tests to assure that measurable, although exaggerated, trends would be obtained.

The factor $2\tan\delta_g$ is involved in the concepts of matchspin and spin mismatch. Match spin is defined as the condition where the nondimensional spin rate is equal to twice the tangent of the serration angle. This, in effect, specifies the spin rate at which the freestream airflow would pass through the serrations without being deflected. For practically all bullets, the axial deceleration is greater than the spin deceleration. Therefore, although the matchspin condition exists near the gun muzzle, down range increasing amounts of overspin occur.

### Results and Discussion

Although these tests on spinning serrated models are somewhat similar to the usual Magnus type, the data obtained on the serrated models are basically different in some respects. Therefore, to avoid confusion, the wind-tunnel data are presented with the usual yaw force and moment coefficient nomenclature and sign convention rather than that typically associated with Magnus data. It should also be kept in mind that, even though the yaw forces and moments act in the horizontal plane, they are caused by model and aerodynamic asymmetries which occur when the model is at an angle of attack in the vertical plane.

A comparison of typical results for the cone-cylinder model with and without serrations is shown in Fig. 2 for tests at a Mach number of 1.5 and a Reynolds number of about $5\times10^6$. Basic differences, as well as similarities are immediately obvious. The curves for the nonserrated model indicate typical Magnus characteristics, i.e.: zero side force at all angles of attack for zero spin; and then approximately linearly increasing side force, for angles of attack other than zero, as the spin rate increases. The serrated model results at zero spin show zero side force only for zero angle of attack. At angles of attack other than zero, the serrated model results indicate a side force even at zero spin. The main cause of this side force at zero spin is apparently due to geometric and aerodynamic asymmetries associated with the serrations when the models are at angle of attack but not the blanking out of the serrations on the lee side of the body since this effect has the opposite sign.

As the spin rate increases, the behavior of the serrated model is very similar to that of the nonserrated model and one sees about the same slopes for corresponding angles of attack. This would suggest that the initial offset, due to asymmetries, is gradually relieved by an opposing Magnus-type force as the model spin increases. At higher spin rates, the side force goes to zero and then changes sign. The significance of the fact that the yaw force goes to zero at a $pd/V$ of approximately 0.4 or about two-thirds of the matchspin condition ($pd/V = 0.628$) is not apparent at this time. It is probably just coincidence that this value is also about the same as that for the experimental free-spin rate shown by the breaks in the curves.

The twist of the serrations on the cone-cylinder model was too great to allow testing up to the matchspin condition. Therefore, the results shown for this model are all in the so-called underspin condition.

The A-N spinner model was considerably different in geometry than the cone-cylinder model but most importantly the twist of the serrations was small enough to provide a matchspin and an overspin capability (matchspin condition, $pd/V = 0.154$). In addition, the model was tested over a wider range of Reynolds numbers. The A-N spinner test results are all for Mach number 2.0. In spite of the differences in model geometry, the characteristics of the A-N spinner data were very similar (for comparable angles of attack and Reynolds number) to those already discussed for the cone-cylinder model.

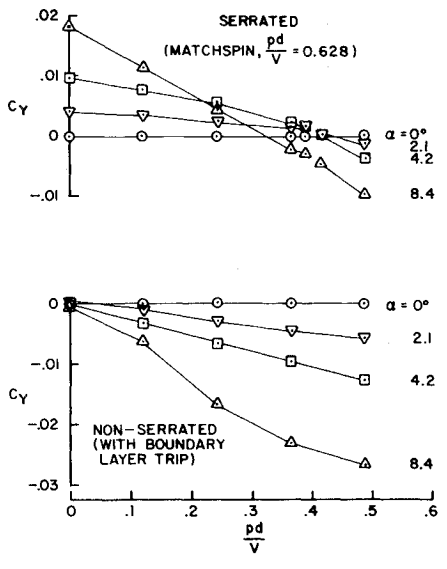


**Fig. 2 Comparison of serrated and nonserrated cone-cylinder results ($M = 1.5$, $Re_l = 5.1\times10^6$).**

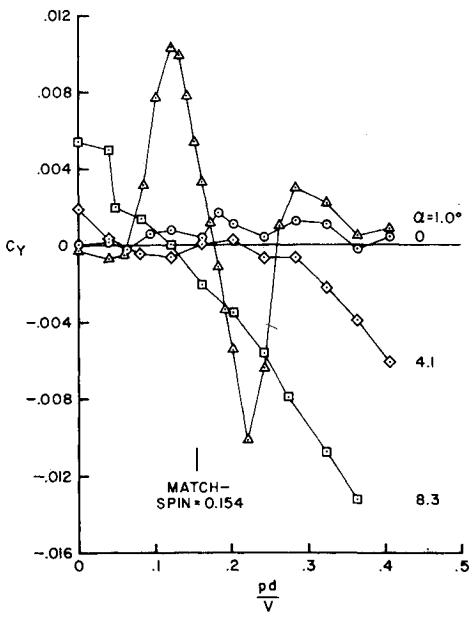


**Fig. 3 Serrated A-N spinner yaw force coefficient data trends ($M = 2.0$, $Re_l = 2\times10^6$).**

Since sea level Reynolds numbers are approximately equal to $1 \times 10^6$ per inch of projectile length at Mach numbers 1.5 and 2.0, the results discussed so far should be pertinent for small caliber projectiles with lengths of about four inches. For smaller projectiles, of small arms size, results at lower Reynolds number should be of more significance.

In Fig. 3, the yaw force coefficient data are shown for a Reynolds number of $2 \times 10^6$. The data trend at the higher angle of attack is similar to that mentioned for the higher Reynolds number. However, at an intermediate angle of attack there is some nonlinearity and at one degree the curve takes the shape of a sine wave. Although not shown, this characteristic shape remains dominant and of significant magnitude even at the lowest angle of attack tested (0.3°). Also, these curves appear to be approximately symmetrical about a point near matchspin. Also of particular significance, considering the fact that the angles of attack are one degree or less, are the relatively large values of yaw force coefficient for small amounts of spin mismatch as well as the extremely steep slopes and sudden slope reversals. Similar trends but with opposite sign occur for negative angles of attack. Increasing the Reynolds number or adding a boundary-layer trip near the nose practically eliminates the strong nonlinearities just discussed.

All of the wind-tunnel test data presented and discussed are for models with rather exaggerated serrations compared to the engraving on a typical bullet. However, the results, although perhaps accentuated, may indicate some of the complexities of the aerodynamics involved for configurations, such as bullets, with more practical departures from mirror symmetry.

### Conclusions

Wind-tunnel tests on spinning models with exaggerated helical serrations have shown that the aerodynamic characteristics can be very complex and quite different than the Magnus characteristics associated with a similar but nonserrated model. Yaw forces and moments occur at angles of attack even at zero spin. As the spin increases, the trends of the yaw forces and moments can be linear at higher angles of attack or very nonlinear at lower angles of attack. The trends are quite sensitive to the Reynolds number and the boundary-layer condition. A strong tendency for symmetry of the data trends about the matchspin condition is noted in some cases, thus, establishing the significance of this parameter. On the basis of these results it is speculated that similar, but more subdued, effects may occur on bullets with less prominent engraving.

### References

[1] Murphy, C. H., "Free Flight Motion of Symmetric Missiles," Ballistic Research Lab. Rept. 1216, July 1963, Aberdeen Proving Ground, Aberdeen, Md.

[2] Sylvester, M. A. and Braun, W. F., "The Influence of Helical Serrations and Bullet Engraving on the Aerodynamic and Stability Properties of a Body of Revolution with Spin," Ballistic Research Lab. Rept. 1514, Nov. 1970, Aberdeen Proving Ground, Aberdeen, Md.

[3] Platou, Anders S., "Magnus Characteristics of Finned and Nonfinned Projectiles," *AIAA Journal*, Vol. 3, No. 1, Jan. 1965, pp. 83–90.

# Vortex-Elliptic Wing Interaction

W. P. JONES*

*Texas A & M University, College Station, Texas*

Received July 26, 1971; revision received September 2, 1971. Work supported by the U.S. Army Research Office—Durham under Project Themis Contract DAHCO4-69-C-0015.

Index category: Airplane and Component Aerodynamics.

*Research Professor, Aerospace Engineering Department. Fellow AIAA.

### Introduction

SEVERAL writers [1-3] have considered the problem of wing-vortex interaction and have obtained approximate solutions by using lifting line theory and purely numerical methods. In this paper, however, the problem is treated analytically and exact solutions have been obtained for different vortex positions relative to the wing. When the vortex is below midspan, solutions for a whole range of aspect ratios can be found once the solution for the lowest aspect ratio has been obtained. In the development of the analysis, it is assumed that the vortex is such that it induces velocities on the wing which are small compared to the mainstream flow so that linearized theory can be used.

### Analysis

As indicated in Fig. 1, the wing is assumed to be of elliptic planform with span $2s$ and mid-chord $2l_o$. The infinite vortex runs parallel to the $OX$ axis and intersects the plane $X = 0$ at $Y_1, h$. Its strength is assumed to be $\gamma(=2\pi U l_o \Gamma)$, where $U$ is the mainstream flow. The upward velocity $w(y)$ induced by the vortex at a section $y$ on the wing is then given by

$$w(y) = U l_o \Gamma (y_1 - y)/[(y_1 - y)^2 + h^2] \tag{1}$$

Since there can be no flow through the wing, an equal and opposite downwash must be created by the vortex induced vorticity distribution generated over the wing. Alternatively, it may be assumed that the effect of the vortex can be represented

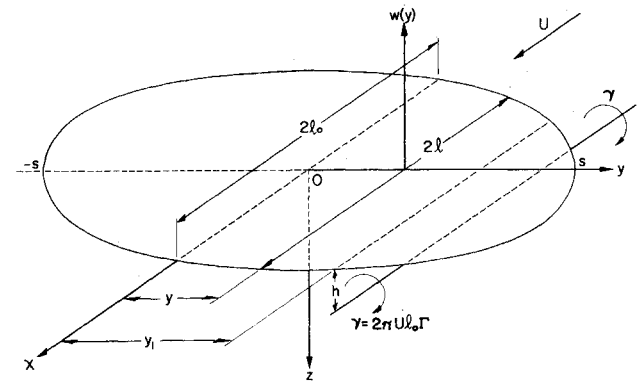


**Fig. 1 Sketch of wing and vortex.**

by assuming the wing to be twisted so that the incidence $\alpha(y)$ at the section $y$ is given by

$$\alpha(y) = \frac{w(y)}{U} = \frac{g\Gamma}{\mu} \frac{(\cos\phi - \cos\phi_1)}{1 + g^2(\cos\phi - \cos\phi_1)^2} \tag{2}$$

where $y = -s\cos\phi$, $g = s/h$ and $\mu = h/l_o$. The problem then reduces to one of determining the distribution of the circulation $K(y)$ corresponding to the mode of effective twist $\alpha(y)$ as defined by Eq. (2). According to lifting line theory, $K(y)$ can then be determined from the equation

$$\alpha(y) = \frac{K(y)}{2\pi U l} + \frac{1}{4\pi U} \int_{-s}^{s} \frac{(\partial K/\partial\eta)\, d\eta}{y - \eta} \tag{3}$$

where $l\ (= l_o \sin\phi)$ is the local semichord. The circulation is assumed to be defined by

$$K(y) = 2\pi U l_0 \Gamma \sum_{n=1}^{\infty} C_n \frac{\sin n\phi}{n} \tag{4}$$

where the $C_n$'s are arbitrary constants to be determined by (3). On substitution of Eq. (4) in (3), the following formula may be obtained, namely

$$\frac{(\cos\phi - \cos\phi_1)\sin\phi}{1 + g^2(\cos\phi - \cos\phi_1)^2} = \sum_{1}^{\infty} A_n \sin n\phi \tag{5}$$